Energy dependence of potential barriers and its effect on fusion cross sections

A. S. Umar,[1] C. Simenel,[2] and V. E. Oberacker[1]
[1]*Department of Physics and Astronomy, Vanderbilt University, Nashville, Tennessee 37235, USA*
[2]*Department of Nuclear Physics, RSPE, Australian National University, Canberra, ACT 0200, Australia*
(Received 28 January 2014; published 12 March 2014)

Background: Couplings between relative motion and internal structures are known to affect fusion barriers by dynamically modifying the densities of the colliding nuclei. The effect is expected to be stronger at energies near the barrier top, where changes in density have longer time to develop than at higher energies. This gives rise to an energy dependence of the barriers as predicted by modern time-dependent Hartree-Fock (TDHF) calculations [K. Washiyama and D. Lacroix, Phys. Rev. C **78**, 024610 (2008)]. Quantitatively, modern TDHF calculations are able to predict realistic fusion thresholds. However, the evolution of the potential barrier with bombarding energy remains to be confronted with the experimental data.
Purpose: The aim is to find signatures of the energy dependence of the barrier by comparing fusion cross-sections calculated from potentials obtained at different bombarding energies with the experimental data.
Method: This comparison is made for the ^{40}Ca+^{40}Ca and ^{16}O+^{208}Pb systems. Fusion cross-sections are computed from potentials calculated with the density-constrained TDHF method.
Results: The couplings decrease the barrier at low-energy in both cases. A deviation from the Woods-Saxon nuclear potential is also observed at the lowest energies. In general, fusion cross-sections around a given energy are better reproduced by the potential calculated at this energy. The coordinate-dependent mass plays a crucial role for the reproduction of sub-barrier fusion cross-sections. Effects of the energy dependence of the potential can be found in experimental barrier distributions only if the variation of the barrier is significant in the energy-range spanned by the distribution. It appears to be the case for ^{16}O+^{208}Pb but not for ^{40}Ca+^{40}Ca.
Conclusions: These results show that the energy dependence of the barrier predicted in TDHF calculations is realistic. This confirms that the TDHF approach can be used to study the couplings between relative motion and internal degrees of freedom in heavy-ion collisions.

DOI: 10.1103/PhysRevC.89.034611 PACS number(s): 21.60.Jz

I. INTRODUCTION

Experimentally obtained fusion cross sections are generally interpreted in terms of models involving a nucleus-nucleus potential barrier, which results from the combination of the attractive nuclear force and the repulsive Coulomb interaction. The reduction of the many-body fusion to a one-dimensional potential barrier problem requires the isolation of the most important physical processes that contribute to the building of the correct effective barrier.

Experimental fusion barrier distributions [1] obtained from the low-energy fusion reactions of heavy-ions shed some light into the detailed microscopic mechanisms that are in play during the entrance channel dynamics on the way to fusion [2,3]. In particular, they may serve as a microscope to discern various inelastic excitations and transfer mechanisms which couple to the relative motion. This coupling to internal degrees of freedom induces a splitting [4] and/or a renormalization of the barrier [5]. The primary underlying mechanism is the dynamical change in the density along the fusion path which modifies the potential energy.

Obviously, this density change is not instantaneous. For instance, it was shown in Ref. [6] that the development of a neck due to couplings to octupole phonons in ^{40}Ca+^{40}Ca could take approximately 1 zs. As a consequence, the dynamical change of the density is most significant at low energy (near the barrier-top) where the colliding partners spend enough time in the vicinity of each other with little relative kinetic energy. At high energies, however, the nuclei overcome the barrier essentially in their ground-state density. This energy dependence of the effect of the couplings on the density evolution was clearly shown in time-dependent Hartree-Fock (TDHF) calculations by Washiyama and Lacroix for the same systems [7]. This naturally translates into an energy dependence of the nucleus-nucleus potential, similar to what was introduced phenomenologically in the Sao-Paulo potential [8]. Consequently, the barrier corresponding to near barrier-top energies includes dynamical couplings effects and can be referred to as a *dynamic-adiabatic* barrier, while at high energy the nucleus-nucleus interaction is determined by a *sudden* potential which can be calculated assuming frozen ground-state densities.

Due to the dynamical nature of this effect time-dependent approaches are well suited for this study. The energy-dependence of the ion-ion potentials have been studied using several approaches based on the fully microscopic TDHF theory [7,9]. It is usually found that the barrier heights increase with bombarding energy. However, this increase is quite slow as the sudden potential is recovered at typically twice (or more) the barrier-top energy [7].

To date, the validity of the TDHF approach in describing the fusion mechanism for heavy-ions has essentially been tested by comparing TDHF fusion thresholds with experimental barriers [6,7,10], although few fusion excitation functions from direct TDHF calculations [10–12] and γ-decay spectra [13] associated to pre-equilibrium giant-dipole resonance [13–16] have also been compared with experimental data. Nevertheless, the agreement between experimental barriers and TDHF

predictions is only for near barrier-top energies, i.e., for the dynamic-adiabatic barrier. Indeed, the predicted transition from the dynamic-adiabatic barrier to the sudden barrier with increasing energy remains to be validated by comparisons with experimental data. The purpose of this study is to accomplish this goal.

Towards this goal, we have calculated fusion cross sections for the ^{40}Ca+^{40}Ca and ^{16}O+^{208}Pb systems using potentials associated with different bombarding energies. These potentials were computed using the density-constrained TDHF (DC-TDHF) method [17] using realistic TDHF trajectories. The comparison of the resulting fusion cross sections with experimental data is used to identify signatures for the energy dependence of the barrier.

In the next section we give a brief outline of the TDHF and DC-TDHF methods used in the calculations. This is followed by the calculation of barriers and fusion cross sections for the ^{40}Ca+^{40}Ca system and subsequently the ^{16}O+^{208}Pb system. The paper ends with the summary and conclusions that can be drawn from the results.

II. THEORETICAL OUTLINE

A. Theoretical tools to describe fusion

Theoretically, the coupled-channels (CC) method is the most commonly used approach to study fusion barriers (see Ref. [18] for a review). The standard CC approach for calculating heavy-ion fusion cross sections contains several adjustable parameters which determine the bare nucleus-nucleus potential which is often assumed to be of Woods-Saxon form. These potential parameters are usually fitted to measured fusion cross sections or to elastic scattering data. In addition, experimental data such as energies and $B(E\lambda)$ values of collective vibrations and giant resonances are required as input for the CC calculations to determine the collective coupling potentials. This is a limitation for exotic nuclei for which these data are not always available. A possible solution of this problem is to compute these parameters directly with microscopic models [6,7,17] and use them in standard coupled channel calculations [6]. Finally, it is difficult to incorporate multinucleon transfer channels into the CC formalism.

Alternatively, fully microscopic theories could be used to overcome these limitations. In particular, they only require an effective interaction or an energy-density functional to describe the interactions between the nucleons. Of course, microscopic approaches are much more time-consuming from a computational point of view and one has to consider approximations to the exact quantum many-body problem. The theoretical formalism for the microscopic description of complex many-body quantum dynamics and the understanding of the nuclear interactions are the underlying challenges for studying low energy nuclear reactions.

B. Time-dependent Hartree-Fock method

The time-dependent Hartree-Fock (TDHF) theory is a mean-field approximation of the exact time-dependent many-body problem. It provides a good starting point for a fully microscopic theory of large amplitude collective motion [19,20] including fusion reactions. But only in recent years has it become feasible to perform TDHF calculations on a three-dimensional Cartesian grid without any symmetry restrictions and with accurate numerical methods [21–27]. In addition, the quality of energy-density functionals has been substantially improved [28–30]. One limitation of the TDHF approach is that it can only be used for fusion at above barrier energies since the theory does not allow for many-body tunneling. Nevertheless, the TDHF fusion threshold provides a prediction of the dynamic-adiabatic barrier-top energy in a very good agreement with experimental data [7,10]. The TDHF theory has then been used to study the couplings between fusion and collective excitations such as rotational motion [31–33] and vibrational modes [6,12–15].

Given a many-body Hamiltonian $\hat{H}$, the action S can be constructed as

$$S = \int_{t_1}^{t_2} dt \langle \Phi(t)|\hat{H} - i\hbar\partial_t|\Phi(t)\rangle. \tag{1}$$

Here, Φ denotes the time-dependent correlated many-body wave function, $\Phi(\mathbf{r_1},\mathbf{r_2},\ldots,\mathbf{r_A};t)$. The variational principle $\delta S = 0$ is then equivalent to the time-dependent Schrödinger equation. In the TDHF approximation the many-body wave function is replaced by a single Slater determinant and this form is preserved at all times. The determinantal form guarantees the antisymmetry required by the Pauli principle for a system of fermions. In this limit, the variation of the action yields the most probable time-dependent mean-field path between points t_1 and t_2 in the multidimensional space-time phase space:

$$\delta S = 0 \rightarrow \Phi_0(t)\ , \tag{2}$$

where $\Phi_0(t)$ is a Slater determinant with the associated single-particle states $\phi_\lambda(\mathbf{r},t)$. The variation in Eq. (2) is performed with respect to the single-particle states ϕ_λ and ϕ^*_λ. This leads to a set of coupled, nonlinear, self-consistent initial value equations for the single-particle states

$$h\left(\{\phi_\mu\}\right)\phi_\lambda = i\hbar\dot{\phi}_\lambda \qquad \lambda = 1,\ldots,N\ , \tag{3}$$

and their Hermitic conjugates. These are the fully microscopic TDHF equations. As we see from Eq. (3), each single-particle state evolves in the mean-field generated by the concerted action of all the other single-particle states.

In standard TDHF applications to heavy-ion collisions, the initial nuclei are calculated using the static Hartree-Fock (HF) theory and the Skyrme functional [28]. The resulting Slater determinants for each nucleus comprise the larger Slater determinant describing the colliding system during the TDHF evolution. Nuclei are assumed to move on a pure Coulomb trajectory until the initial separation between the nuclear centers used in TDHF evolution. Of course, no assumption is made on the subsequent trajectory in the TDHF evolution. Using the Coulomb trajectory we compute the relative kinetic energy at this separation and the associated translational momenta for each nucleus. The nuclei are then boosted by multiplying the HF states with

$$\Phi_j \rightarrow \exp(\imath\mathbf{k}_j\cdot\mathbf{R})\Phi_j\ , \tag{4}$$

where Φ_j is the HF state for nucleus j and $\mathbf{R}$ is the corresponding center of mass coordinate

$$\mathbf{R} = \frac{1}{A_j}\sum_{i=1}^{A_j}\mathbf{r}_i \ . \tag{5}$$

The Galilean invariance and the conservation of the total energy in the Skyrme TDHF equations are used to check the convergence of the calculations.

Due to the fact that TDHF calculations do not include sub-barrier tunneling of the many-body wave function, the fusion probability, $P_{\rm fus}(L, E_{\rm c.m.})$, for a particular orbital angular momentum L at the center-of-mass energy $E_{\rm c.m.}$ can only be $P_{\rm fus}^{\rm TDHF} = 0$ or 1. As a consequence the quantal expression for the fusion cross-section

$$\sigma_{\rm fus}(E_{\rm c.m.}) = \frac{\pi\hbar^2}{2\mu E_{\rm c.m.}}\sum_{L=0}^{\infty}(2L+1)P_{\rm fus}(L, E_{\rm c.m.}) \ , \tag{6}$$

where μ is the reduced mass of the system, reduces to

$$\begin{aligned}\sigma_{\rm fus}(E_{\rm c.m.}) &= \frac{\pi\hbar^2}{2\mu E_{\rm c.m.}}\sum_{L=0}^{L_{\rm max}(E_{\rm c.m.})}(2L+1) \\ &= \frac{\pi\hbar^2}{2\mu E_{\rm c.m.}}[L_{\rm max}(E_{\rm c.m.})+1]^2 \ , \end{aligned} \tag{7}$$

$L_{\rm max}$ being the largest orbital angular momentum leading to fusion. This is known as the quantum sharp cut-off formula [34].

Since TDHF is based on the independent-particle approximation it can be interpreted as the semiclassical limit of a fully quantal theory thus allowing a connection to macroscopic coordinates and providing insight about the collision process. In this sense the TDHF dynamics can only be used to compute the semiclassical trajectories of the collective moments of the composite system as a function of time. Note that the part of the residual interaction which is neglected in TDHF may produce fluctuations and correlations which affect these trajectories. Recent beyond TDHF developments have been used to investigate the effects of such fluctuations in heavy-ion collisions [35,36]. However, the TDHF approach is optimized to the expectation values of one-body operators [37] and is then capable to predict these quantities. This was demonstrated by the recent successes of TDHF in reproducing various reaction mechanisms in heavy-ion collisions. Moreover, beyond TDHF calculations remain numerically difficult. We then restrict the present calculations to the TDHF level.

One of the main application of recent TDHF codes has been to study fusion reactions. For TDHF collisions of light and medium mass systems, as well as highly mass-asymmetric systems, fusion generally occurs immediately above the Coulomb barrier. In heavier systems, however, there is an energy range above the barrier where fusion does not occur [20,38,39]. This phenomenon is the microscopic analog of the macroscopic *extra-push* threshold [40]. In the extreme case of actinide collisions, fusion becomes impossible and the fragments reseparate in a few zeptoseconds [41–43].

The path to fusion as described in TDHF calculations is a sequence of states from dinuclear configurations to a compact compound system. Along this path, one-body dissipation plays a crucial role and single-particle friction can quickly absorb the kinetic energy of the relative motion. As long as the average single-particle excitation energy per nucleon is less than the shell energy (about 4–8 MeV) the details of the ground state potential energy surface are still felt and shell correction energies influence the TDHF dynamics. It is precisely for this reason that the DC-TDHF approach allows us to reproduce ion-ion interaction barriers for heavy-ion collisions.

C. DC-TDHF method

The TDHF theory does not include quantum tunneling of the many-body wave function. Consequently, direct TDHF calculations cannot be used to describe sub-barrier fusion. Nevertheless, a number of approaches based on TDHF were developed to extract fusion potentials with dynamical effects [7,17] in order to compute fusion cross sections at sub-barrier energies.

The density-constrained TDHF (DC-TDHF) utilizes a novel approach of using time-dependent densities from TDHF to self-consistently calculate the underlying ion-ion interaction potentials [17] and excitation energies [44]. These potential barriers then allow for the calculation of fusion cross sections at both sub-barrier and above-barrier energies. The method was applied to calculate fusion and capture cross sections above and below the barrier, ranging from light systems [12,45] to hot and cold fusion reactions leading to superheavy element $Z = 112$ [39]. In all cases a good agreement between the measured fusion cross sections and the DC-TDHF results was found. This is rather remarkable given the fact that the only input in TDHF is the Skyrme energy-density functional whose parameters are determined from structure information.

The concept of using density as a constraint for calculating collective states from TDHF time-evolution was first introduced in Ref. [46], and used in calculating collective energy surfaces in connection with nuclear molecular resonances in Ref. [47]. In this approach the TDHF time-evolution takes place with no restrictions. At certain times during the evolution the instantaneous density is used to perform a static Hartree-Fock minimization while holding the neutron and proton densities constrained to be the corresponding instantaneous TDHF densities. In essence, this provides us with the TDHF dynamical path in relation to the multi-dimensional static energy surface of the combined nuclear system. The advantages of this method in comparison to other mean-field based microscopic methods such as the constrained Hartree-Fock (CHF) method are obvious. First, there is no need to introduce external constraining operators which assume that the collective motion is confined to the constrained phase space. Second, the static adiabatic approximation is replaced by the dynamical analog where the most energetically favorable state is obtained by including sudden rearrangements and the dynamical system does not have to move along the valley of the potential energy surface. In short we have a self-organizing system which selects its evolutionary path by itself following the microscopic dynamics. All of the dynamical features included in TDHF are naturally included in the DC-TDHF calculations. These effects include neck

formation, mass exchange, internal excitations, deformation effects to all order, as well as the effect of nuclear alignment for deformed systems.

In the DC-TDHF method the ion-ion interaction potential is given by

$$V_{\rm DC}(R) = E_{\rm DC}(R) - E_{A_1} - E_{A_2}\ , \tag{8}$$

where $E_{\rm DC}$ is the density-constrained energy at the instantaneous separation $R(t)$, while E_{A_1} and E_{A_2} are the binding energies of the two nuclei obtained with the same effective interaction. This ion-ion potential $V_{\rm DC}(R)$ is asymptotically correct since at large initial separations it exactly reproduces $V_{\rm Coulomb}(R_{\rm max})$. In addition to the ion-ion potential it is also possible to obtain coordinate dependent mass parameters. One can compute the "effective mass" $M(R)$ using the conservation of energy

$$M(R) = \frac{2[E_{\rm c.m.} - V_{\rm DC}(R)]}{\dot{R}^2}\ , \tag{9}$$

where the collective velocity $\dot{R}$ is directly obtained from the TDHF evolution. This coordinate dependent mass can be exactly incorporated into the ion-ion potential, which we call $V(R)$, by using a point-transformation [48,49]. The effect of the coordinate-dependent mass is to modify the inner part of the ion-ion potential, which is important for fusion cross sections at deep sub-barrier energies.

Fusion cross sections are calculated by directly integrating the Schrödinger equation

$$\left[\frac{-\hbar^2}{2\mu}\frac{d^2}{dR^2} + \frac{\hbar^2\ell(\ell+1)}{2\mu R^2} + V(R) - E_{\rm c.m.}\right]\psi_\ell(R) = 0\ , \tag{10}$$

using the well-established incoming wave boundary condition (IWBC) method [50] to obtain the barrier penetrabilities $P_{\rm fus}(L, E_{\rm c.m.})$ which determine the total fusion cross section [Eq. (6)].

In writing Eq. (8) we have introduced the concept of an adiabatic reference state for a given TDHF configuration. The adiabatic reference state is the one obtained via the density constraint calculation. It is the Slater determinant with lowest energy for the given density with vanishing current. It is then used to approximate the collective potential energy [46]. We would like to emphasize that this procedure does not affect the TDHF time-evolution and contains no free parameters or normalization.

Finally, ion-ion interaction potentials calculated using DC-TDHF correspond to the configuration attained during a particular TDHF collision. For light and medium mass systems as well as heavier systems for which fusion is the dominant reaction product, DC-TDHF calculations at near barrier-top energy give a fusion barrier which is expected to match the TDHF fusion threshold. In practice, due to the underlying numerical approximations in the DC-TDHF method, small (typically less than 0.5 MeV) underestimation of the TDHF fusion threshold are sometime observed.

III. RESULTS

TDHF calculations for the DC-TDHF computation of microscopic potential barriers for the ^{40}Ca+^{40}Ca system were done in a Cartesian box which is 50 fm along the collision axis and 25 fm in the other two directions. The nuclei were placed at an initial separation of 20 fm. For the ^{16}O+^{208}Pb system we have chosen a Cartesian box which is 60 fm along the collision axis and 30 fm in the other two directions. The two nuclei are placed at an initial separation of 24 fm. Calculations used the SLy4 Skyrme functional [28] as described in Ref. [26]. Static calculations are done using the damped-relaxation method [51]. The numerical accuracy of the static binding energies and the deviation of the computed DC-TDHF potential from the point Coulomb energy in the initial state of the collision dynamics is of the order of 50–150 keV. We have performed density constraint calculations at every 10–20 fm/c interval.

A. ^{40}Ca+^{40}Ca fusion barriers

Recently, particular experimental attention has been given to fusion reactions involving Ca isotopes [52–55]. These new experiments supplement older fusion data [56] and extend them to lower sub-barrier energies. In Ref. [55] a comprehensive CC calculation for this system has also been presented utilizing the *shallow potential* approach [57]. These calculations use M3Y+repulsion potential and the excitations of collective phonons. In particular, octupole vibrations have been shown to play an important role on the dynamics in this system [6,58].

1. Nucleus-nucleus potentials

The ^{40}Ca+^{40}Ca system was investigated in Ref. [59] with the DC-TDHF method using TDHF c.m. energies 55, 60, and 65 MeV. The resulting potential barriers are reported in Fig. 1. In the present work, additional calculations have been performed to study in more details the energy dependence

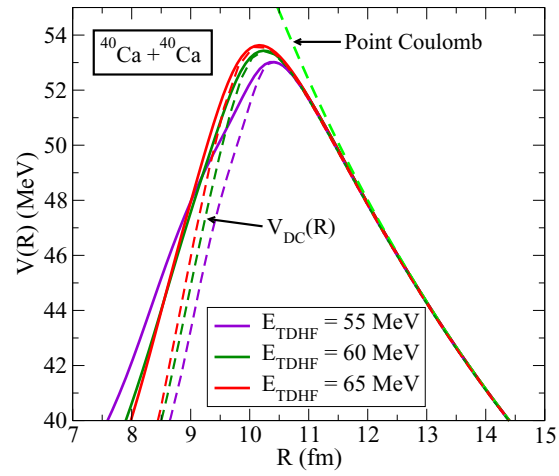

FIG. 1. (Color online) DC-TDHF ion-ion interaction potentials $V(R)$ (solid lines) including coordinate dependence of the effective mass $M(R)$ for ^{40}Ca+^{40}Ca obtained from TDHF calculations at various center-of-mass energies. The potentials $V_{\rm DC}(R)$ obtained without the coordinate dependence of $M(R)$ are plotted with thin dashed lines. The barrier peaks shift up with increasing energy. Shown also is the corresponding point-Coulomb potential (thick dashed line).

of the barrier and its effect on the fusion cross sections. We have performed TDHF calculations in 1 MeV intervals in the 53–65 MeV range and computed the corresponding DC-TDHF potentials. As a result, barrier heights are in the range of 52.6–53.6 MeV all located in the vicinity of nuclear separation $R = 10.2$ fm. We observe that for the ^{40}Ca+^{40}Ca system DC-TDHF potential barriers do not show an apparent strong energy dependence.

In the DC-TDHF method the energy dependence of the barriers arises from the changing dynamical behavior of the system. At energies close to the barrier-top the onset of neck dynamics is slow and allow ample time for density rearrangements for the system, whereas as the energy is increased there is less and less time for rearrangements to occur and a long-lived neck to form, thus approaching the frozen-density limit [7]. The barrier corresponding to the lowest TDHF energy may be called the *dynamic-adiabatic* barrier as opposed to a *static-adiabatic* barrier that could be obtained by using the constrained Hartree-Fock approach or a prescription like the folding model. The barrier corresponding to TDHF energies much higher than the dynamic-adiabatic barrier may be labeled as the *sudden* barrier. We see from Fig. 1 that this leads to an increasing barrier height with increasing collision energy and quickly saturates for energies that are considerably higher than the lowest energy barrier. In this sense, we obtain a distribution of barriers as a function of collision energy.

An important dynamical effect is due to the coordinate-dependence of the mass, $M(R)$. In Fig. 1 this effect is demonstrated by plotting the direct DC-TDHF potentials, $V_{\rm DC}(R)$ (dashed lines), and those that include the modification of the coordinate-dependent mass, $V(R)$ (solid lines). For TDHF collisions of symmetric systems the net particle transfer is zero and cannot affect $M(R)$. However, the dynamical neck formation and collective excitations are possible and can change the effective mass.

The potentials shown in Fig. 1 should not be directly compared with nucleus-nucleus potentials entering CC calculations. Indeed, the latter are uncoupled potentials with various couplings and particle transfer added on subsequently. In cases were double-folding method is used the densities are frozen as the nuclear separation R changes. This usually implies a higher uncoupled barrier height as it was found to be in the range 54.1–54.7 MeV in Refs. [6,7,55,60].

2. *Fusion cross sections*

The corresponding fusion cross sections calculated from the potentials $V(R)$ shown in Fig. 1 are plotted in Fig. 2 in logarithmic scale and in Fig. 3 in linear scale. The experimental points are from Refs. [55,56]. The cross sections clearly depend on the TDHF energy used to extract the DC-TDHF potential. The interaction potential corresponding to the lowest TDHF energy leads to fusion cross sections which are in good agreement with the sub-barrier fusion data but overestimate the cross sections at higher energies. On the other hand, the potential corresponding to the highest energy reproduces the highest energy data but underestimates the data at lower energies.

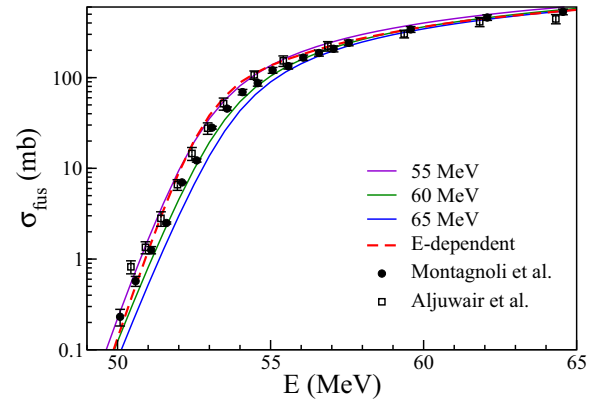

FIG. 2. (Color online) Fusion cross sections for ^{40}Ca+^{40}Ca obtained from the DC-TDHF potentials shown in Fig. 1. The dashed line represents the combined cross sections $\bar{\sigma}(E)$. The data points are from Refs. [55,56]. DC-TDHF curves shift down with increasing energy.

In principle, each set of cross sections $\sigma_n(E)$ is valid only near the TDHF energy E_n used to calculate the potential. One can then generate a unique function $\bar{\sigma}(E) = \sum_n \sigma_n(E) f_n(E)$ where $f_n(E)$ is a weighting function peaked at $E = E_n$. In practice, $\bar{\sigma}(E)$ has been generated using

$$f_0 = \begin{cases} 1 & E < E_0 \\ \cos^2\left[\frac{\pi}{2}\,\frac{E-E_0}{\Delta E}\right] & E_0 \leqslant E \leqslant E_1 \\ 0 & E > E_1 \end{cases}$$

$$f_{0<n<N} = \begin{cases} 0 & E < E_{n-1} \\ \cos^2\left[\frac{\pi}{2}\,\frac{E-E_n}{\Delta E}\right] & E_{n-1} \leqslant E \leqslant E_{n+1} \\ 0 & E > E_{n+1} \end{cases}$$

$$f_N = \begin{cases} 0 & E < E_{N-1} \\ \cos^2\left[\frac{\pi}{2}\,\frac{E-E_N}{\Delta E}\right] & E_{N-1} \leqslant E \leqslant E_N \\ 1 & E > E_N \end{cases} .$$

E_0 is the lowest TDHF energy at which fusion is observed and from which a potential can be extracted, while E_N is the maximum TDHF energy considered in this work. ΔE

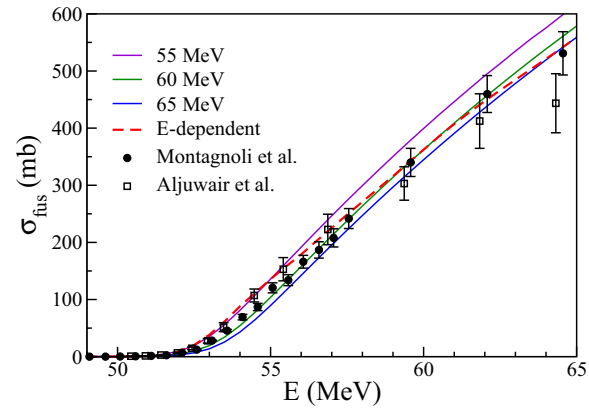

FIG. 3. (Color online) Same as Fig. 2 in linear vertical scale. DC-TDHF curves shift down with increasing energy.

is the constant energy step in the TDHF calculations. (The generalization to nonconstant ΔE is trivial.)

The resulting $\bar{\sigma}(E)$ is labeled "E-dependent" in Figs. 2 and 3. Considering the experimental error bars and the fluctuations between the data sets, we see that there is an overall agreement between $\bar{\sigma}(E)$ and the experimental fusion cross sections, despite a slight overestimation of the more recent data from Ref. [55] in the barrier region. It is then reassuring to observe that the energy-dependent DC-TDHF potentials lead to reasonable reproduction of the data in the energy-range of the TDHF energy used for their calculation. This comparison with experimental data also confirms that the potential barrier "seen" by the system at high energy is effectively higher than the one at low energy. It is unfortunate, however, that this energy dependence cannot be investigated below the barrier. This is due to the fact that the TDHF calculations at sub-barrier energies do not lead to fusion and, then, the DC-TDHF method cannot be applied to extract the potential in this energy regime. Nevertheless, the good agreement between sub-barrier data and the theoretical cross sections calculated with the dynamic-adiabatic potential indicates that this energy dependence is likely to be small.

3. Fusion barrier distributions

To investigate possible signatures of the energy dependence at energies close to the barrier, we have calculated the following quantity [3]:

$$D(E_i) = \left[\frac{d^2(E\sigma_{\rm fus}(E))}{dE^2}\right]_i \simeq \left(\frac{(E\sigma)_{i+1} - 2(E\sigma)_i - (E\sigma)_{i-1}}{\Delta E^2}\right), \quad (11)$$

which is known as the fusion barrier distribution [1]. It is essentially zero except in the energy range of the barrier and has then been widely used to study the effect of the couplings between relative motion and internal structures on fusion barriers. As it was discussed in some detail in Ref. [3] the calculation of the barrier distribution using the above formula is sensitive to the value of the energy separation ΔE used in the finite-difference formula. Commonly, a value between $\Delta E = 1$–2 MeV is used.

Selected barrier distributions obtained from different TDHF energies are shown in Fig. 4 together with experimental data from Refs. [55,56]. The barrier distributions were calculated with $\Delta E = 1$ MeV. The distributions corresponding to different TDHF energies are generally smooth but the centroids shift to a higher energy with increasing TDHF energy and the heights of the distributions become lower. This change can be interpreted as being due to the difference in the dynamical processes that are more prevalent at barrier-top energies in comparison to higher energies where we approach the frozen-density limit. Despite fluctuations in the experimental data, it is clear that the distributions associated with the high TDHF energies ($E_{\rm TDHF} = 60$ and 65 MeV) do not reproduce the experimental barrier distribution. This is of course not a problem as the comparison should be made at energies close to 60–65 MeV, for which $D(E) \simeq 0$. Nevertheless, this indicates

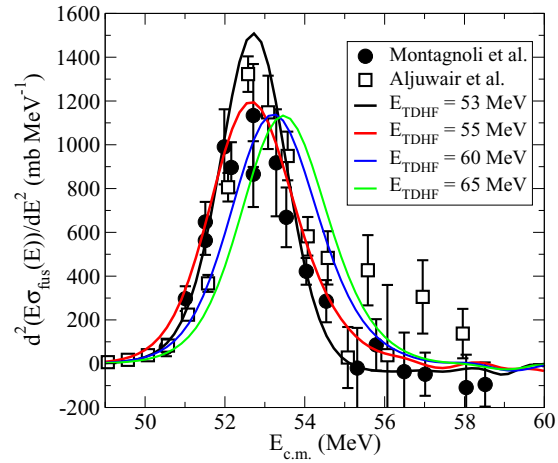

FIG. 4. (Color online) Fusion barrier distributions for ^{40}Ca+^{40}Ca obtained from DC-TDHF potentials calculated with different TDHF energies. DC-TDHF barrier distributions shift down and to the right with increasing energy. The data shown as solid-filled circles are from Ref. [55], and the squares are from Ref. [56].

that the measured barrier distributions provide information on the dynamic-adiabatic barrier, but not on the potential seen by the system at higher energies.

B. ^{16}O+^{208}Pb fusion barriers

The second system we have studied is ^{16}O+^{208}Pb. The choice of this system is partly motivated by the fact that its fusion barrier is affected by early charge equilibration dynamics [10,61]. Quantitative reproductions of fusion cross sections for this system would then be an indication that the TDHF approach is able to treat the interplay between nucleon transfer and fusion. This system is also one for which fusion hindrance at deep sub-barrier energies has been observed [62]. Standard coupled-channels calculations including low lying vibrational states and one-neutron transfer channels could not consistently reproduce the high and low-energy fusion data. While the shallow-potential approach of Ref. [57] had some success in reproducing the low-energy part of the data it required an imaginary potential to reproduce the high-energy part of the data. Furthermore, inconsistencies in the shallow-potential approach for simultaneously reproducing the low and high-energy fusion data was pointed out in Ref. [62].

1. Nucleus-nucleus potentials

We have performed TDHF calculations in 1 MeV intervals between 75 and 80 MeV center-of-mass energies, as well as at 90 and 100 MeV. The corresponding DC-TDHF barriers are shown in Fig. 5 for $E_{\rm TDHF} = 75$, 80, and 100 MeV. Barrier heights are in the range of 73.7–75.0 MeV all located in the vicinity of nuclear separation $R = 12$ fm. As it was in the previous study the barrier thickness at sub-barrier energies changes with changing collision energy due to the fact that at lower energies the system has more time to rearrange its density, which would manifest itself as the formation of a neck followed by nucleon transfer [7,10,63] and collective

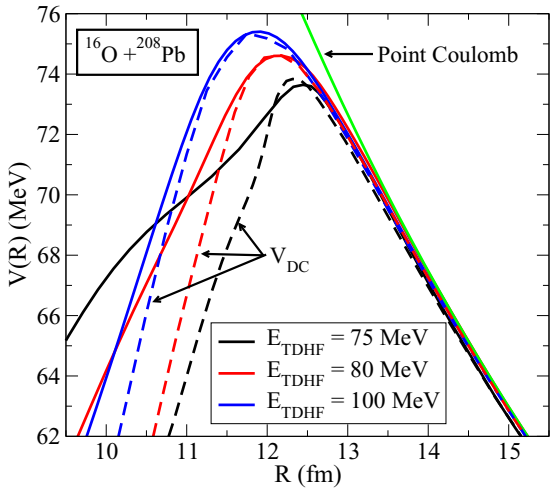

FIG. 5. (Color online) DC-TDHF ion-ion interaction potential $V(R)$ (solid lines) including coordinate dependence of the effective mass $M(R)$ for ^{16}O+^{208}Pb obtained from TDHF calculations at various center-of-mass energies. The potentials $V_{DC}(R)$ obtained without the coordinate dependence of $M(R)$ are plotted with thin dashed lines. The barrier peaks shift up with increasing energy. Shown also is the corresponding point-Coulomb potential.

excitations. Similarly, the energy of the barrier-top is highest for highest energy approaching the sudden limit at high energies. Moreover, we observe that as we move down from the potential peak the inner part of the barrier usually deviates from the Woods-Saxon+Coulomb form, which is the case for deep sub-barrier energies, with or without the coordinate-dependent mass.

In Ref. [64] a method was developed to extract the ion-ion potential directly from the experimental sub-barrier cross sections in an attempt to understand the reason for CC calculations not reproducing sub-barrier and high-energy part of the data with a single potential model. These calculations showed that the form of the potential deviated from the Woods-Saxon shape and one of the possible reasons to account for this deviation was suggested to be the coordinate-dependent mass. The potential barrier extracted directly from the sub-barrier data was called the *adiabatic* potential and is plotted in Fig. 6 (solid line, the shaded region indicates uncertainty) together with the DC-TDHF potential at 75 MeV with (dashed line) and without (dotted line) the coordinate-dependent mass. The potential with coordinate dependent mass is in much better agreement with the one extracted from data using the inversion method. We can conclude from these calculations that indeed the coordinate-dependent mass, which is really a byproduct of heavy-ion and neck dynamics, is largely responsible for the thickening of the barrier for deep sub-barrier energies as shown in Fig. 5.

2. *Fusion cross sections*

As in the ^{40}Ca+^{40}Ca reaction, the energy dependence of the ion-ion interaction potentials observed in Fig. 5 leads to the corresponding change in the calculated fusion cross sections as shown in Figs. 7 (logarithmic scale) and 8 (linear

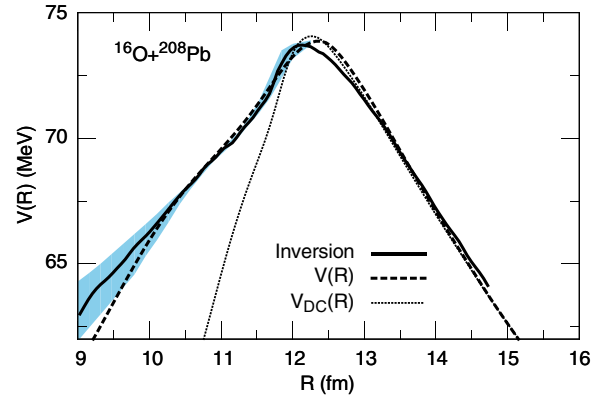

FIG. 6. (Color online) The *adiabatic* potential obtained in Ref. [64] compared with the DC-TDHF potential reproducing the sub-barrier cross sections.

scale). Also shown in the same figures are the experimental cross sections from Refs. [65]. The general trends observed in the energy-dependence of the cross sections is similar to the ^{40}Ca+^{40}Ca case. Indeed, the potential obtained at the lowest TDHF energy reproduces the sub-barrier cross sections. In addition, the experimental cross sections at high energy are better reproduced by potentials calculated at similar energies. However, it is noticeable that, even in the energy range where they are supposed to be valid, the energy-dependent potential overestimates the experimental data. Note that this is not a drawback of the method used to extract the potential as the problem can be traced back to the TDHF approximation itself. Indeed, direct TDHF cross sections computed at above barrier energies by finding the maximum impact parameter for fusion at each energy overestimate the experimental cross sections by the same amount (see Fig. 8). As the TDHF calculations reproduce well the centroid of the experimental barrier distribution [7,10], it is then likely that beyond mean-field effects are responsible for the observed discrepancy above

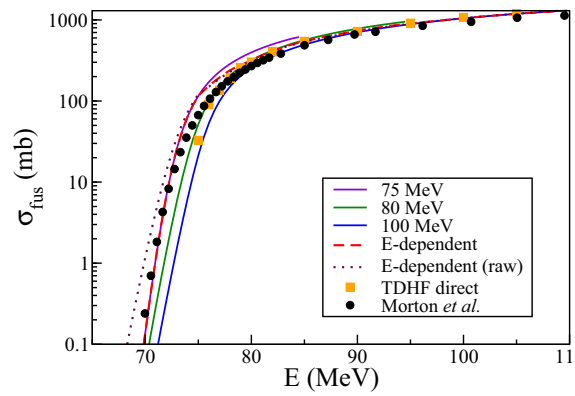

FIG. 7. (Color online) Fusion cross sections for ^{16}O+^{208}Pb obtained from the DC-TDHF potentials shown in Fig. 5. The dashed and dotted lines represent the combined cross sections $\bar{\sigma}(E)$ obtained with and without coordinate dependent mass, respectively. DC-TDHF curves shift down with increasing energy. The data points are from Ref. [65].

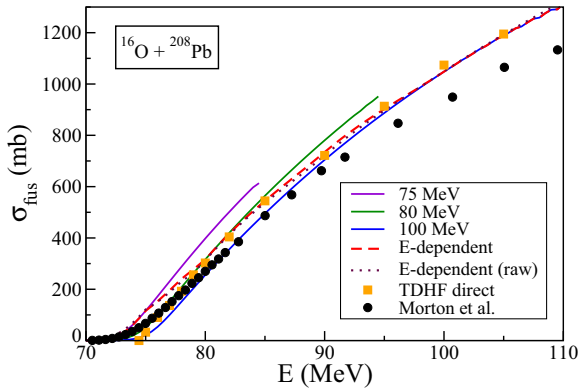

FIG. 8. (Color online) Same as Fig. 7 in linear vertical scale. DC-TDHF curves shift down with increasing energy.

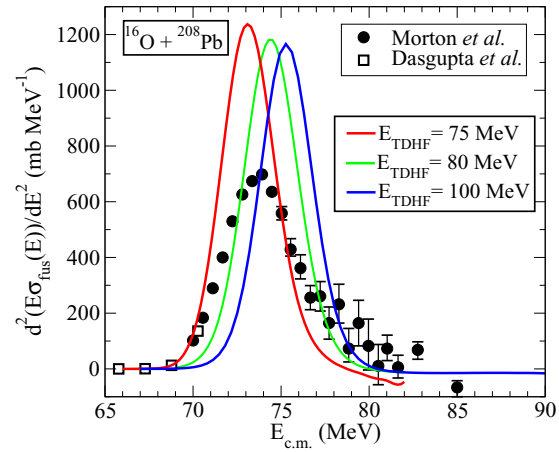

FIG. 9. (Color online) Fusion barrier distributions for ^{16}O+^{208}Pb obtained for various TDHF energies. The data shown as solid-filled circles are from Refs. [62,65]. DC-TDHF barrier distributions shift to the right with increasing energy.

the barrier. For instance, the transfer of a proton pair, and, to a lesser extent, of an α cluster, which are not included in TDHF calculations, have been shown to be an important mechanism in this system [66,67]. Nevertheless, this discrepancy is relatively small considering the fact that there are no free parameters.

Let us now investigate the effect of the coordinate dependence of the effective mass $M(R)$ on the fusion cross sections. In Figs. 7 and 8 we have also plotted the calculated E-dependent cross sections without the use of the coordinate-dependent mass (dotted curve). Figure 8 shows that, above the barrier, the inclusion of the coordinate dependence of the effective mass does not play an important role as both energy-dependent calculations lead to similar cross sections. However, Fig. 7 shows that this is not the case below the barrier. Here, the effect of $M(R)$ on the low-energy cross section is seen to be essential. Indeed, without the coordinate dependence of the mass, the cross sections are overestimated below the barrier. Including this dependence widens the barrier (see Fig. 5) and consequently reduces the cross sections, providing a much better agreement with the data (see Fig. 7).

3. *Fusion barrier distributions*

Finally, we study the effect of the energy dependence of the potential on the fusion barrier distribution $D(E)$. So far, standard CC calculations have not been able to reproduce the fusion barrier distributions consistently for low and high energies [65]. Improved barrier distributions at lower energies were calculated using CC with the shallow-potential method [57]. However, above barrier cross sections could only be explained with addition of an imaginary absorbing potential. We have constructed fusion-barrier distributions from the DC-TDHF cross section by using an energy spacing of $\Delta E = 2.0$ MeV as shown in Fig. 9 for TDHF bombarding energies 75, 80, and 100 MeV. Also shown are the data from Refs. [62,65]. A first observation is that the DC-TDHF barrier distributions suffer from the overestimation of the barrier distributions at intermediate energies. The difficulty in reproducing this region is shared with standard CC approaches. The origin of this discrepancy are still unclear. Another observation is that, as the TDHF energy is increased, the corresponding distributions peak at higher energies. This qualitative observation was also made in the ^{40}Ca+^{40}Ca case. In addition, each theoretical barrier distribution is narrower than the experimental one. This observation could be attributed to the energy dependence of the potential. Indeed, the high energy tail of the experimental barrier distribution extends up to ~80 MeV. The barrier distribution computed from the $E_{\rm TDHF} = 75$ MeV potential naturally fails to reproduce the high energy part of the experimental barrier distribution. The latter is much better reproduced by the $E_{\rm TDHF} = 80$ MeV potential. The tail in the 75–80 MeV region can then be interpreted as an effect of the gradual increase of the barrier height in this energy range. Note that this effect is not visible in the ^{40}Ca+^{40}Ca data due to the fact that the change in barrier height is not noticeable in the limited energy range span by the barrier distribution.

IV. SUMMARY AND DISCUSSION

Ion-ion potentials are sensitive to the excitation and transfer mechanism in play on the way to forming a compound nucleus. However, these couplings between relative motion and internal degrees of freedom have time to affect the nucleus-nucleus potential only at low energy, leading to a "dynamic-adiabatic" potential. At high energy, the system does not have enough time to rearrange its density, leading to a "sudden" potential. As a result, this leads to an energy dependence of the potential and, in particular, of its barrier. The purpose of this work was to identify signatures of this energy dependence in experimental fusion cross sections by comparing with the predictions of microscopic calculations.

Fusion potentials around the barrier have been calculated for the ^{40}Ca+^{40}Ca and ^{16}O+^{208}Pb systems using the DC-TDHF method based on TDHF density evolutions. It is shown that, as we go to above barrier energies, the energy dependence of the potential increases the barrier height and consequently slows down the increase of the fusion cross sections with increasing bombarding energy. This effect happens in a large energy range until the sudden potential is reached (according to Ref. [7], this can occur at about twice the energy of the barrier).

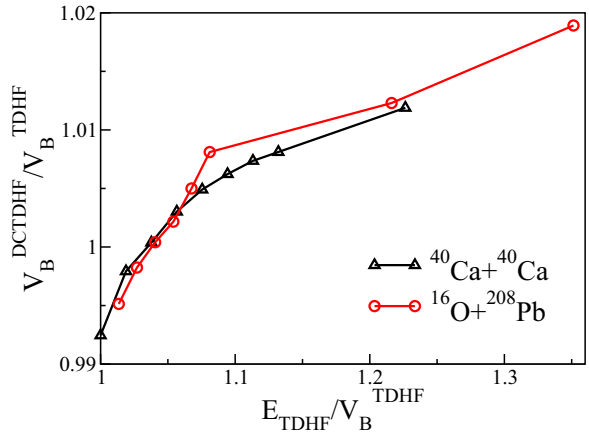

FIG. 10. (Color online) The ratio of barrier heights obtained from DC-TDHF and direct TDHF calculations plotted against the dimensionless scale variable $E_{\rm TDHF}/V_B^{\rm TDHF}$.

As a result, the dynamic-adiabatic and the sudden barriers can be very different. The former reproduces sub-barrier data, while the latter provides a better agreement at well above barrier energies than at low energies. Discrepancies remain, however, at above barrier energies for the ^{16}O+^{208}Pb system, which could be due to proton-pair and α-cluster transfer not included in the theory. It should also be noted that signatures of the energy dependence of the potential are less visible in the experimental barrier distributions due to the fact that these distributions usually span a small energy range in which the variation of the barrier is not always very sensitive.

Finally, let us compare the energy-dependence of the potentials in both systems. This is done in Fig. 10 where we plot the ratio of the barrier heights obtained from DC-TDHF, $V_B^{\rm DC-TDHF}$, and direct TDHF, $V_B^{\rm TDHF}$, calculations as a function of the dimensionless variable $E_{\rm TDHF}/V_B^{\rm TDHF}$. It is interesting to note that the energy dependence of the barriers are found to be very similar for both systems. It is then not surprising that the same behavior is obtained in the fusion cross-section plots.

The quality of the results suggests that the mean-field dynamics present in TDHF does properly account for many of the excitation and transfer mechanisms. Naturally, this is achieved in an average way as opposed to a fully quantal theory. The present calculations are another testament to a growing number of TDHF calculations, both in the small amplitude limit for low-lying and collective state calculations and in the large amplitude limit of reaction dynamics, finding good comparisons with experimental observations. This progress is partially due to the increased computational capabilities that allow such calculations to be performed without using any symmetry restrictions and with modern energy density functionals. This suggests that for low-energy heavy-ion reactions TDHF remains as an ever more useful theoretical tool.

ACKNOWLEDGMENTS

Useful discussions with M. Dasgupta and D. J. Hinde are acknowledged. This work has been supported by the US Department of Energy under Grant No. DE-FG02-96ER40975 with Vanderbilt University, and by the Australian Research Council under Grants No. FT120100760, FL110100098, and DP1094947. Part of the calculations have been performed on the NCI National Facility in Canberra, Australia, which is supported by the Australian Commonwealth Government.

[1] N. Rowley, G. Satchler, and P. Stelson, Phys. Lett. B **254**, 25 (1991).
[2] J. R. Leigh, M. Dasgupta, D. J. Hinde, J. C. Mein, C. R. Morton, R. C. Lemmon, J. P. Lestone, J. O. Newton, H. Timmers, J. X. Wei, and N. Rowley, Phys. Rev. C **52**, 3151 (1995).
[3] M. Dasgupta, D. J. Hinde, N. Rowley, and A. M. Stefanini, Ann. Rev. Nucl. Part. Sci. **48**, 401 (1998).
[4] C. Dasso, S. Landowne, and A. Winther, Nucl. Phys. A **432**, 495 (1985).
[5] K. Hagino, N. Takigawa, M. Dasgupta, D. J. Hinde, and J. R. Leigh, Phys. Rev. Lett. **79**, 2014 (1997).
[6] C. Simenel, M. Dasgupta, D. J. Hinde, and E. Williams, Phys. Rev. C **88**, 064604 (2013).
[7] K. Washiyama and D. Lacroix, Phys. Rev. C **78**, 024610 (2008).
[8] L. C. Chamon, B. V. Carlson, L. R. Gasques, D. Pereira, C. De Conti, M. A. G. Alvarez, M. S. Hussein, M. A. Cândido Ribeiro, E. S. Rossi, Jr., and C. P. Silva, Phys. Rev. C **66**, 014610 (2002).
[9] V. E. Oberacker, A. S. Umar, J. A. Maruhn, and P.-G. Reinhard, Phys. Rev. C **82**, 034603 (2010).
[10] C. Simenel and B. Avez, Int. J. Mod. Phys. E **17**, 31 (2008).
[11] P. Bonche, B. Grammaticos, and S. Koonin, Phys. Rev. C **17**, 1700 (1978).
[12] C. Simenel, R. Keser, A. S. Umar, and V. E. Oberacker, Phys. Rev. C **88**, 024617 (2013).
[13] C. Simenel, P. Chomaz, and G. de France, Phys. Rev. C **76**, 024609 (2007).
[14] C. Simenel, P. Chomaz, and G. de France, Phys. Rev. Lett. **86**, 2971 (2001).
[15] V. E. Oberacker, A. S. Umar, J. A. Maruhn, and P.-G. Reinhard, Phys. Rev. C **85**, 034609 (2012).
[16] A. S. Umar and V. E. Oberacker, Phys. Rev. C **71**, 034314 (2005).
[17] A. S. Umar and V. E. Oberacker, Phys. Rev. C **74**, 021601(R) (2006).
[18] K. Hagino and N. Takigawa, Prog. Theor. Phys. **128**, 1001 (2012).
[19] J. W. Negele, Rev. Mod. Phys. **54**, 913 (1982).
[20] C. Simenel, Eur. Phys. J. A **48**, 152 (2012).
[21] P.-G. Reinhard, A. S. Umar, K. T. R. Davies, M. R. Strayer, and S. J. Lee, Phys. Rev. C **37**, 1026 (1988).
[22] A. S. Umar, M. R. Strayer, J. S. Wu, D. J. Dean, and M. C. Guclu, Phys. Rev. C **44**, 2512 (1991).
[23] K.-H. Kim, T. Otsuka, and P. Bonche, J. Phys. G **23**, 1267 (1997).

[24] J. A. Maruhn, P. G. Reinhard, P. D. Stevenson, J. R. Stone, and M. R. Strayer, Phys. Rev. C **71**, 064328 (2005).
[25] T. Nakatsukasa and K. Yabana, Phys. Rev. C **71**, 024301 (2005).
[26] A. S. Umar and V. E. Oberacker, Phys. Rev. C **73**, 054607 (2006).
[27] L. Guo, J. A. Maruhn, P.-G. Reinhard, and Y. Hashimoto, Phys. Rev. C **77**, 041301(R) (2008).
[28] E. Chabanat, P. Bonche, P. Haensel, J. Meyer, and R. Schaeffer, Nucl. Phys. A **635**, 231 (1998).
[29] P. Klüpfel, P.-G. Reinhard, T. J. Büervenich, and J. A. Maruhn, Phys. Rev. C **79**, 034310 (2009).
[30] M. Kortelainen, T. Lesinski, J. More, W. Nazarewicz, J. Sarich, N. Schunck, M. V. Stoitsov, and S. Wild, Phys. Rev. C **82**, 024313 (2010).
[31] C. Simenel, P. Chomaz, and G. de France, Phys. Rev. Lett. **93**, 102701 (2004).
[32] A. S. Umar and V. E. Oberacker, Phys. Rev. C **74**, 024606 (2006).
[33] A. S. Umar and V. E. Oberacker, Phys. Rev. C **77**, 064605 (2008).
[34] J. S. Blair, Phys. Rev. **95**, 1218 (1954).
[35] C. Simenel, Phys. Rev. Lett. **106**, 112502 (2011).
[36] K. Washiyama, S. Ayik, and D. Lacroix, Phys. Rev. C **80**, 031602(R) (2009).
[37] R. Balian and M. Véneroni, Phys. Rev. Lett. **47**, 1353 (1981).
[38] Lu Guo and Takashi Nakatsukasa, EPJ Web Conf. **38**, 09003 (2012).
[39] A. S. Umar, V. E. Oberacker, J. A. Maruhn, and P.-G. Reinhard, Phys. Rev. C **81**, 064607 (2010).
[40] W. J. Swiatecki, Nucl. Phys. A **376**, 275 (1982).
[41] J. Tian, X. Wu, K. Zhao, Y. Zhang, and Z. Li, Phys. Rev. C **77**, 064603 (2008).
[42] C. Golabek and C. Simenel, Phys. Rev. Lett. **103**, 042701 (2009).
[43] D. J. Kedziora and C. Simenel, Phys. Rev. C **81**, 044613 (2010).
[44] A. S. Umar, V. E. Oberacker, J. A. Maruhn, and P.-G. Reinhard, Phys. Rev. C **80**, 041601(R) (2009).
[45] A. S. Umar, V. E. Oberacker, and C. J. Horowitz, Phys. Rev. C **85**, 055801 (2012).
[46] R. Y. Cusson, P.-G. Reinhard, M. R. Strayer, J. A. Maruhn, and W. Greiner, Z. Phys. A **320**, 475 (1985).
[47] A. S. Umar, M. R. Strayer, R. Y. Cusson, P.-G. Reinhard, and D. A. Bromley, Phys. Rev. C **32**, 172 (1985).
[48] K. Goeke, F. Grümmer, and P.-G. Reinhard, Ann. Phys. (NY) **150**, 504 (1983).
[49] A. S. Umar and V. E. Oberacker, Eur. Phys. J. A **39**, 243 (2009).
[50] K. Hagino, N. Rowley, and A. T. Kruppa, Comput. Phys. Commun. **123**, 143 (1999).
[51] C. Bottcher, M. R. Strayer, A. S. Umar, and P.-G. Reinhard, Phys. Rev. A **40**, 4182 (1989).
[52] A. M. Stefanini, G. Montagnoli, R. Silvestri, L. Corradi, S. Courtin, E. Fioretto, B. Guiot, F. Haas, D. Lebhertz, P. Mason, F. Scarlassara, and S. Szilner, Phys. Lett. B **679**, 95 (2009).
[53] C. L. Jiang, A. M. Stefanini, H. Esbensen, K. E. Rehm, L. Corradi, E. Fioretto, P. Mason, G. Montagnoli, F. Scarlassara, R. Silvestri, P. P. Singh, S. Szilner, X. D. Tang, and C. A. Ur, Phys. Rev. C **82**, 041601(R) (2010).
[54] G. Montagnoli, F. Scarlassara, P. Mason, A. M. Stefanini, R. Silvestri, L. Corradi, E. Fioretto, B. Guiot, S. Courtin, F. Haas, D. Lebhertz, and S. Szilner, Nucl. Phys. A **834**, 159c (2010).
[55] G. Montagnoli, A. M. Stefanini, C. L. Jiang, H. Esbensen, L. Corradi, S. Courtin, E. Fioretto, A. Goasduff, F. Haas, A. F. Kifle, C. Michelagnoli, D. Montanari, T. Mijatović, K. E. Rehm, R. Silvestri, P. P. Singh, F. Scarlassara, S. Szilner, X. D. Tang, and C. A. Ur, Phys. Rev. C **85**, 024607 (2012).
[56] H. A. Aljuwair, R. J. Ledoux, M. Beckerman, S. B. Gazes, J. Wiggins, E. R. Cosman, R. R. Betts, S. Saini, and O. Hansen, Phys. Rev. C **30**, 1223 (1984).
[57] H. Esbensen and S. Misicu, Phys. Rev. C **76**, 054609 (2007).
[58] N. Rowley and K. Hagino, Nucl. Phys. A **834**, 110c (2010).
[59] R. Keser, A. S. Umar, and V. E. Oberacker, Phys. Rev. C **85**, 044606 (2012).
[60] S. Misicu and F. Carstoiu, Phys. Rev. C **84**, 051601(R) (2011).
[61] C. Simenel, Phys. Rev. Lett. **105**, 192701 (2010).
[62] M. Dasgupta, D. J. Hinde, A. Diaz-Torres, B. Bouriquet, C. I. Low, G. J. Milburn, and J. O. Newton, Phys. Rev. Lett. **99**, 192701 (2007).
[63] A. S. Umar, V. E. Oberacker, and J. A. Maruhn, Eur. Phys. J. A **37**, 245 (2008).
[64] K. Hagino and Y. Watanabe, Phys. Rev. C **76**, 021601(R) (2007).
[65] C. R. Morton, A. C. Berriman, M. Dasgupta, D. J. Hinde, J. O. Newton, K. Hagino, and I. J. Thompson, Phys. Rev. C **60**, 044608 (1999).
[66] F. Videbæk, R. B. Goldstein, L. Grodzins, S. G. Steadman, T. A. Belote, and J. D. Garrett, Phys. Rev. C **15**, 954 (1977).
[67] M. Evers, M. Dasgupta, D. J. Hinde, D. H. Luong, R. Rafiei, R. du Rietz, and C. Simenel, Phys. Rev. C **84**, 054614 (2011).